

Synthesis, Structure, and Molecular Dynamics of Gallium Complexes of Schizokinen and the Amphiphilic Siderophore Acinetoferrin

Evgeny A. Fadeev, Minkui Luo, and John T. Groves*

Contribution from the Department of Chemistry, Princeton University,
Princeton, New Jersey 08544

Received March 31, 2004; E-mail: jtgroves@princeton.edu

Abstract: A new general synthesis of the citrate-based siderophores acinetoferrin (**Af**) and schizokinen (**Sz**) and their analogues is described. The molecular structure of gallium schizokinen, Ga**Sz**, was determined by combined ^1H NMR, Hartree–Fock ab initio calculations, DFT, and empirical modeling of vicinal proton NMR spin–spin couplings. The metal-coordination geometry of Ga**Sz** was determined from NOE contacts to be *cis-cis* with respect to the two chelating hydroxamates. One diaminopropane adopts a single chairlike conformation while another is a mixture of two ring pucker arrangements. Both amide hydrogens are internally hydrogen bonded to metal-ligating oxygen atoms. The acyl methyl groups are directed away from each other with an average planar angle of ca. 130° . The kinetics of Ga**Sz** racemization were followed by selective, double spin–echo inversion–recovery ^1H NMR spectroscopy over the temperature range of 10 – 45°C . The racemization proceeds by a multistep mechanism that is proton independent between pD 5 and 12 ($k_0 = 1.47$ (0.15 s^{-1})) and acid catalyzed below pD 4 ($k_1 = 2.25$ (0.15) $\times 10^4\text{ M}^{-1}\text{ s}^{-1}$). The activation parameters found for the two sequential steps of the proton independent pathway were $\Delta H^\ddagger = 25 \pm 3\text{ kcal M}^{-1}$, $\Delta S^\ddagger = 25 \pm 7\text{ cal M}^{-1}\text{ K}^{-1}$ and $\Delta H^\ddagger = 17.1 \pm 0.2\text{ kcal M}^{-1}$, $\Delta S^\ddagger = 0.3 \pm 2.7\text{ cal M}^{-1}\text{ K}^{-1}$. The first step of the proton-independent mechanism was assigned to the dissociation of the carboxyl group. The second step was assigned to complex racemization. The proton-assisted step was assigned to a complete dissociation of the α -hydroxy carboxyl group at pD < 4 . The ab initio modeling of gallium acinetoferrin, Ga**Af**, and analogues derived from the structure of Ga**Sz** has shown that the pendant *trans*-octenoyl fragments are oriented in opposite directions with the average planar angle of ca. 130° . This arrangement prevents Ga**Af** from adopting a phospholipid-like structural motif. Significantly, iron siderophore complex Fe**Af** was found to be disruptive to phospholipid vesicles and is considerably more hydrophilic than **Af**, with an eight-fold smaller partition coefficient.

Introduction

Siderophores are a class of low molecular weight organic compounds that are produced by microorganisms in response to iron deficiency. These compounds are capable of highly selective chelation and delivery of inorganic iron^{1,2} to bacterial cells via specific, receptor-mediated membrane transport mechanisms.³ Siderophore-mediated iron uptake is an important determinant of bacterial growth³ and there is suggestive evidence that iron proteins and siderophores are involved in cell signaling cascades and quorum sensing.^{4–6} Amphiphiles are a significant and widely distributed subset of siderophores,⁷ having been found in pathogens,^{8–11} terrestrial symbionts,¹² and marine

microorganisms.^{13–15} Mycobactins, lipophilic siderophores of *Mycobacter smegmatis*, have shown beneficial activity for the treatment of arteriosclerosis,¹⁶ breast cancer,¹⁷ and postischemic reperfusion injury.¹⁸ A synthetic, amphiphilic analogue of desferoxamine has been reported to inhibit malaria^{19,20} and another lipophilic tripeptide ornithine-based hydroxamate

- (1) Albrecht-Gary, A. M.; Crumbliss, A. L. *Met. Ions Biol. Syst.* **1998**, *35*, 239–327.
- (2) Boukhalfa, H.; Crumbliss, A. L. *Biometals* **2002**, *15*, 325–339.
- (3) Neilands, J. B. *J. Biol. Chem.* **1995**, *270*, 26723–26726.
- (4) Fong, K. P.; Gao, L.; Demuth, D. R. *Infect. Immun.* **2003**, *71*, 298–308.
- (5) Zhu, J.; Dizin, E.; Hu, X.; Wavreille, A.; Park, J.; Pei, D. *Biochemistry* **2003**, *42*, 4717–4726.
- (6) Bollinger, N.; Hasset, D. J.; Iglewski, B. H.; Costerton, J. W.; McDermott, T. R. *J. Bacteriol.* **2001**, *183*, 1990–1996.
- (7) Groves, J. T. *Proc. Natl. Acad. Sci. U.S.A.* **2003**, *100*, 3569–3574.
- (8) Lane, S. J.; Marshall, P. S.; Upton, R. J.; Ratledge, C. *Biometals* **1998**, *11*, 13–20.

- (9) Okujo, N.; Sakakibara, Y.; Yoshida, T.; Yamamoto, S. *Biometals* **1994**, *7*, 170–176.
- (10) Snow, G. A. *Biochem. J.* **1965**, *97*, 166–175.
- (11) Snow, G. A. *Biochem. J.* **1965**, *94*, 160–165.
- (12) Persmark, M.; Pittman, P.; Buyer, J. S.; Schwyn, B.; Gill, P. R.; Neilands, J. B. *J. Am. Chem. Soc.* **1993**, *115*, 3950–3956.
- (13) Macrellis, H. M.; Trick, C. G.; Rue, E. L.; Smith, G.; Bruland, K. W. *Mar. Chem.* **2001**, *76*, 175–187.
- (14) Butler, A.; Martinez, J. S.; Barbeau, K. J. *Inorg. Biochem.* **2001**, *86*, 30–30.
- (15) Martinez, J. S.; Zhang, G. P.; Holt, P. D.; Jung, H. T.; Carrano, C. J.; Haygood, M. G.; Butler, A. *Science* **2000**, *287*, 1245–1247.
- (16) Rosenthal, E. A.; Bohlmeier, T. J.; Monnet, E.; MacPhail, C.; Robertson, A. D.; Horwitz, M. A.; Burchenal, J. E. B.; Horwitz, L. D. *Circulation* **2001**, *104*, 2222–2227.
- (17) Pahl, P. M. B.; Horwitz, M. A.; Horwitz, K. B.; Horwitz, L. D. *Breast Cancer Res. Treat.* **2001**, *69*, 69–79.
- (18) Horwitz, L. D.; Sherman, N. A.; Kong, Y. N.; Pike, A. W.; Gobin, J.; Fennessey, P. V.; Horwitz, M. A. *Proc. Natl. Acad. Sci. U.S.A.* **1998**, *95*, 5263–5268.
- (19) Lytton, S. D.; Cabantchik, Z. I.; Libman, J.; Shanzer, A. *Mol. Pharmacol.* **1991**, *40*, 584–590.

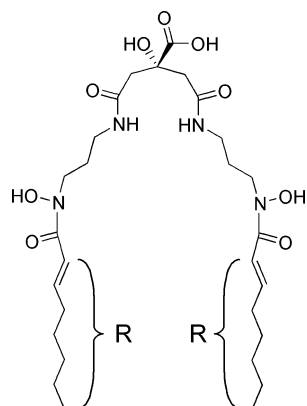


Figure 1. Structure of acinetoferrin, **Af** ($R = \text{trans-1-heptenyl}$) and **Sz** ($R = \text{methyl}$).

chelator was found to effectively promote growth of *Mycobacter smegmatis*.²¹ Strategies for the design of antibiotic “Trojan Horse” siderophore conjugates have been described.²² The ubiquity of amphiphilic siderophores, the mechanisms of their exploitation by pathogens, and their promising pharmacological activities focus attention on the structures and functions of these little-studied natural products.

Our interest in amphiphiles²³ and membrane assemblies^{24–27} has led us to examine the citrate-based siderophore acinetoferrin (**Af**) of *Acinetobacter haemolyticus*, an antibiotic-resistant bacterium that causes an increasing number of difficult-to-treat infections.²⁸ This bacterium produces two siderophores: acinetoferrin⁹ (principally) and smaller amounts of acinetobactin.^{29,30} Acinetoferrin belongs to a class of citrate-based siderophores (Figure 1) in which the terminal carboxyl groups of citric acid are peptide-coupled to two hydroxamate-bearing appendages. Other citrate-based siderophores are aerobactin,³¹ arthrobactin,³² nannochelin,³³ petrobactin,^{34–36} rhizobactin 1021,¹² and schizokinen (**Sz**).^{37–39}

Acinetoferrin is a unique member of this family, having two lipophilic side chains resembling a phospholipid structural motif. The amphiphilic nature of this siderophore and its unusual structure are suggestive of a special mechanism of action,

wherein its interactions with cell membranes play an essential role. While the coordination chemistry of ferric schizokinen **FeSz**⁴⁰ and ferric aerobactin⁴¹ have been investigated spectroscopically, no molecular structures of this class of citrate-based siderophores have been reported.

Here we present an efficient and general synthesis of **Af**, **Sz**, and their analogues. We also describe the three-dimensional structure of the Ga^{3+} complexes of **Sz** and **Af** derived from ¹H NMR data, Hartree–Fock ab initio, and DFT molecular modeling. The coordination geometries of the **GaAf** and **GaSz** hydroxamate groups are unambiguously determined to be *cis-cis*. The two enantiomers of **GaAf** and **GaSz** are shown by ¹H NMR to equilibrate readily. A sequential, two-step mechanism of racemization has been discerned from the kinetics of this process. The solution structure of **FeAf** and the conformational analysis of the **FeAf** aliphatic tails have been inferred from the **GaSz** geometry. The resulting conformation of **FeAf** suggests a special mode of interaction of the metal-**Af** complex with the cell phospholipid membranes that is dictated by a change in the arrangement of the lipophilic side chains upon metal binding.

Results

Synthesis of Siderophores. Synthesis of schizokinen⁴² and acinetoferrin⁴³ were reported previously. We developed a general method (Figure 2) allowing synthetic access to both compounds and their 2-E-butenoyl and 2-E-dodecenoyl homologues without major changes in the procedure. The key feature of this approach is the coupling of 2-*tert*-butyl-1,3-di-*N*-(hydroxy)succinimidyl citrate,⁴² **1**, with 1-*N*-benzoyloxy-1,3-diaminopropane dihydrochloride **2**. Compound **2** was conveniently obtained from *N*-(3-(*tert*-butoxycarbonylamino)-*N*-(1-benzoyloxy)-diaminopropane⁴³ upon treatment with dry HCl.

Attachment of the acyl fragments to **3** was achieved in high yield via the appropriate acyl chloride. The resulting fully protected siderophores, **4a–d**, were amenable to purification by column chromatography under conditions dictated by the terminal acyl chain length. This strategy has the advantage of retaining the protected hydroxamate groups until the molecular scaffold was fully assembled, thus lessening the iron contamination acquired from the glassware and silica that is an inherent difficulty with these compounds.⁴³

The benzoyl protecting groups of **4a–d** were removed under basic conditions and the resulting crude products were separated on a short column packed with a specially prepared, iron-free silica.⁴³ Final cleavage of the *tert*-butyl esters **5a–c** was effected with 95:5 TFA:H₂O at 25 °C. We found that dry TFA led to some dehydration of the citrate hydroxyl. The free siderophores **6a** (**Sz**) and **6c** were purified by gel filtration with sephadex G-10. Compounds **6b** (**Af**) and **6d** were sufficiently lipophilic to be separated from the residual TFA by the chloroform/water extraction.

Stoichiometry and Overall Structure of the Iron **Af and Gallium **Sz** Complexes.** The iron complexes **Fe-6(a–d)** were prepared by metalation of **6(a–d)** with ferric ammonium citrate. Polyacrylamide gel electrophoresis showed that **Fe-6(a–d)** were

- (20) Harpstrite, S. E.; Beatty, A. A.; Collins, S. D.; Oksman, A.; Goldberg, D. E.; Sharma, V. *Inorg. Chem.* **2003**, *42*, 2294–2300.
 (21) Lin, Y. M.; Miller, M. J.; Mollmann, U. *Biomaterials* **2001**, *14*, 153–157.
 (22) Murray, A. P.; Miller, M. J. *J. Org. Chem.* **2003**, *68*, 191–194.
 (23) Xu, G. F.; Martinez, J. S.; Groves, J. T.; Butler, A. *J. Am. Chem. Soc.* **2002**, *124*, 13408–13415.
 (24) Lahiri, J.; Fate, G. D.; Ungashe, S. B.; Groves, J. T. *J. Am. Chem. Soc.* **1996**, *118*, 2347–2358.
 (25) Groves, J. T.; Fate, G. D.; Lahiri, J. *J. Am. Chem. Soc.* **1994**, *116*, 5477–5478.
 (26) Groves, J. T.; Neumann, R. *J. Am. Chem. Soc.* **1989**, *111*, 2900–2909.
 (27) Groves, J. T.; Neumann, R. *J. Am. Chem. Soc.* **1987**, *109*, 5045–5047.
 (28) Rudant, E.; Courvalin, P.; Lambert, T. *Antimicrob. Agents Chemother.* **1997**, *41*, 2646–2651.
 (29) Yamamoto, S.; Okujo, N.; Sakakibara, Y. *Arch. Microbiol.* **1994**, *162*, 249–254.
 (30) Dorsey, C. W.; Tolmasky, M. E.; Crosa, J. H.; Actis, L. A. *Microbiology* **2003**, *149*, 1227–1238.
 (31) Gibson, F.; Magrath, D. I. *Biochim. Biophys. Acta* **1969**, *192*, 175–184.
 (32) Schaffit, M.; Diekmann, H. *Arch. Microbiol.* **1978**, *117*, 203–207.
 (33) Kunze, B.; Trowitzschkianast, W.; Hofle, G.; Reichenbach, H. *J. Antibiot.* **1992**, *45*, 147–150.
 (34) Barbeau, K.; Zhang, G.; Live, D. H.; Butler, A. *J. Am. Chem. Soc.* **2002**, *124*, 378–379.
 (35) Bergeron, R. J.; Huang, G. F.; Smith, R. E.; Bharti, N.; McManis, J. S.; Butler, A. *Tetrahedron* **2003**, *59*, 2007–2014.
 (36) Gardner, R. A.; Kinkade, R.; Wang, C. J.; Phanstiel, O. *J. Org. Chem.* **2004**, *69*, 3530–3537.
 (37) Akers, H. A. *Appl. Environ. Microbiol.* **1983**, *45*, 1704–1706.
 (38) Simpson, F. B.; Neilands, J. B. *J. Physiol.* **1976**, *12*, 44–48.
 (39) Trick, C. G.; Kerry, A. *Curr. Microbiol.* **1992**, *24*, 241–245.

- (40) Plowman, J. E.; Loehr, T. M.; Goldman, S. J.; Sanders-Loehr, J. *J. Inorg. Biochem.* **1984**, *20*, 183–197.
 (41) Harris, W. R.; Carrano, C. J.; Raymond, K. N. *J. Am. Chem. Soc.* **1979**, *101*, 2722–2727.
 (42) Milewska, M. J.; Chimiak, A.; Glowacki, Z. *J. Prakt. Chem./Chem.-Ztg.* **1987**, *329*, 447–456.
 (43) Wang, Q. X.; Phanstiel, O. I. *J. Org. Chem.* **1998**, *63*, 1491–1495.

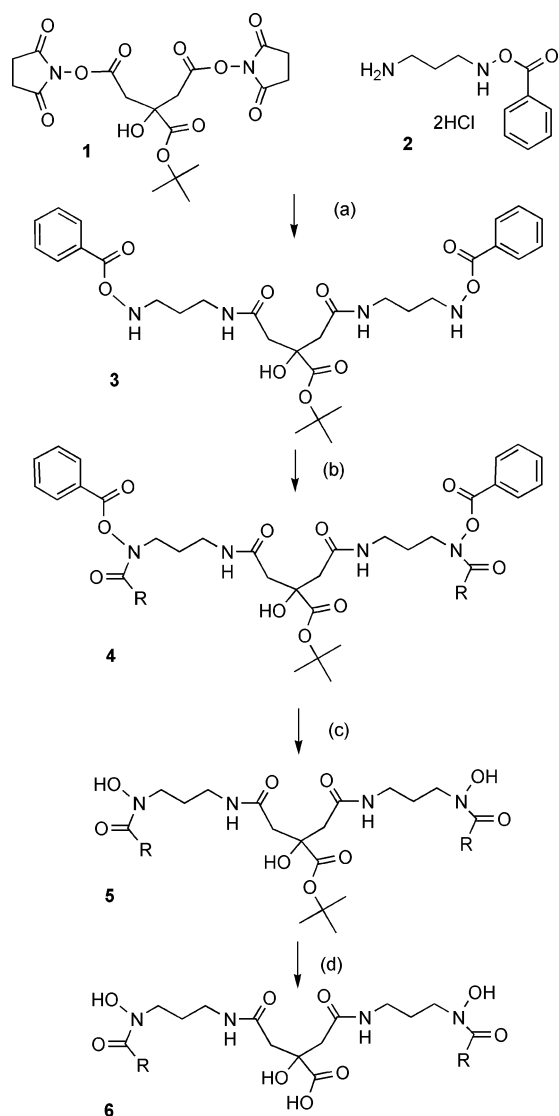


Figure 2. General synthesis of the acinetoferrin siderophore family: (a) 3 equiv of TEA, CH₃CN; (b) 2 equiv of acyl chloride, CH₂Cl₂, reflux, 1 h; (c) 2 equiv of 5 N aqueous NaOH, CH₃OH, 0 °C, 10 min; (d) TFA/H₂O 19:1, 1 h. **R:** -CH₃- **4-6a**; *trans*-(CH₂)₂(CH₂)₄CH₃- **4-6b**; *trans*-(CH₂)₂CH₃- **4-6c**; *trans*-(CH₂)₂(CH₂)₈CH₃- **4-6d**.

negatively charged at neutral pH. Orange colored bands ($\lambda_{\text{max}} = 400\text{--}426\text{ nm}$) of the complex molecules were observed to move toward the anode. Negative ion electrospray mass spectrometry of FeAf and GaSz (Figures S1 and S2) complexes showed one major peak at m/z 636 and 485, respectively, corresponding to a 1:1 metal–siderophore complex bearing one negative charge. A NMR titration of Sz with GaBr₃ (Figure S3) also indicated a 1:1 metal-to-ligand stoichiometry in agreement with the conclusions of Plowman et al.⁴⁰ for the FeSz complex. Therefore, the ligands must saturate the Ga³⁺ and Fe³⁺ octahedral coordination and the α -hydroxy acid as well as the two hydroxamates are deprotonated.

NMR Spectroscopy of GaSz. The ¹H NMR spectra of GaSz (Figure 3) and GaAf (Figure S16) were very similar, indicating very similar structures. Among the spectral similarities are the ordering and shape of the ¹H signals from the citrate and 1,3-diaminopropane methylene groups, and the presence of the two NOE cross-peaks between *one* methylene proton adjacent to the each hydroxamate and the vinyl (GaAf) or methyl (GaSz)

protons of the terminal alkyl side chains. The GaSz spectrum was more amenable to detailed analysis as it was better resolved and not complicated by the presence of signals from the *trans*-octenoyl fragments of GaAf.

The ¹H NMR spectrum of the Na[GaSz] in D₂O (Figure 3) displayed remarkably well-defined multiplets in the range of δ 1.4–4.3 for the methylene and methyl protons and at δ 7.5 and 9.3 for the amide protons. There were additional broad resonances more pronounced at higher pH (>6) that were not assigned to a particular structure and probably account for a partially hydrolyzed complex.

The ¹H peaks of the terminal methyl groups and all the methylene hydrogen atoms, excluding those on the citrate moiety, were assigned to one of the *N-n*-diaminopropane branches on the ligand on the basis of the bond connectivity revealed by COSY and distance via NOESY spectra. Thus, resonances 1–7 in Figure 3 belong to one diaminopropane chain (designated *chain I*), and resonances 1'–7' to the other chain (*chain II*). Resonances from the methylene groups neighboring the hydroxamate residues (2, 2', 4, and 4') were distinguished by the presence of the NOE correlation peaks between the resonances 2 and 2' with the corresponding terminal methyl protons. Hydrogen atoms on the methylene groups connected to the amide nitrogens were identified by observing crosspeaks in the COSY spectrum with WET water resonance suppression.

The ¹H resonance chemical shift assignments for GaSz and the spin–spin coupling values are shown in Table 1. The observed spin-coupling pattern for *chain I* is consistent with a single conformation with well-defined, staggered relationship of the central methylene (resonances 6 and 7) with the two neighboring methylene groups (resonances 2–5). Resonance 7 clearly originates from a proton bearing two *trans*-diaxial relationships with its neighbors. Also, there is an additional NOE signal (not observed for the *chain II*) between the two hydrogen atoms (resonances 4 and 5) separated by three carbon atoms. The protons in *chain II*, by contrast, display more average-sized vicinal splittings. Also, the chemical shift dispersion within geminal proton pairs is smaller in the *chain II*.

That every proton in the molecule has a distinctive chemical shift indicated that the GaSz complex is chiral. The 1D ¹H NMR spectra of GaSz and GaAf did not show signs of exchange broadening at room temperature but NOE spectra (Figures S15 and S16) showed slow exchange of *chain I* and *chain II* resonances, indicating that the chains interchanged their identities by the racemization.⁴⁴ The racemization kinetics were followed by a Double Pulsed Field Gradient Spin–Echo (DPFGSE) NOESY-1D experiment⁴⁵ that has a great advantage over 2D NOESY measurements for small molecules due to the higher accuracy and speed. The kinetic data yielded accurate racemization rate constants and activation parameters (see the section below) allowing an insight into the racemization mechanism.

Another interesting feature of the GaSz NMR data is the low-field values of the amide hydrogen chemical shifts (resonances 1 and 1') at δ 9.43 and 7.5, suggesting the presence of intramolecular hydrogen bonds.⁴⁶ To investigate properties of

(44) Perrin, C. L.; Dwyer, T. J. *Chem. Rev.* **1989**, *90*, 935–967.

(45) Stott, K.; Keeler, J.; Van, Q. N.; Shaka, A. J. *J. Magn. Reson.* **1997**, *125*, 302–324.

(46) Becker, E. Hydrogen bonding. In *Encyclopedia of Nuclear Magnetic Resonance*; John Wiley: New York, 1996; Vol. 4, p 4212.

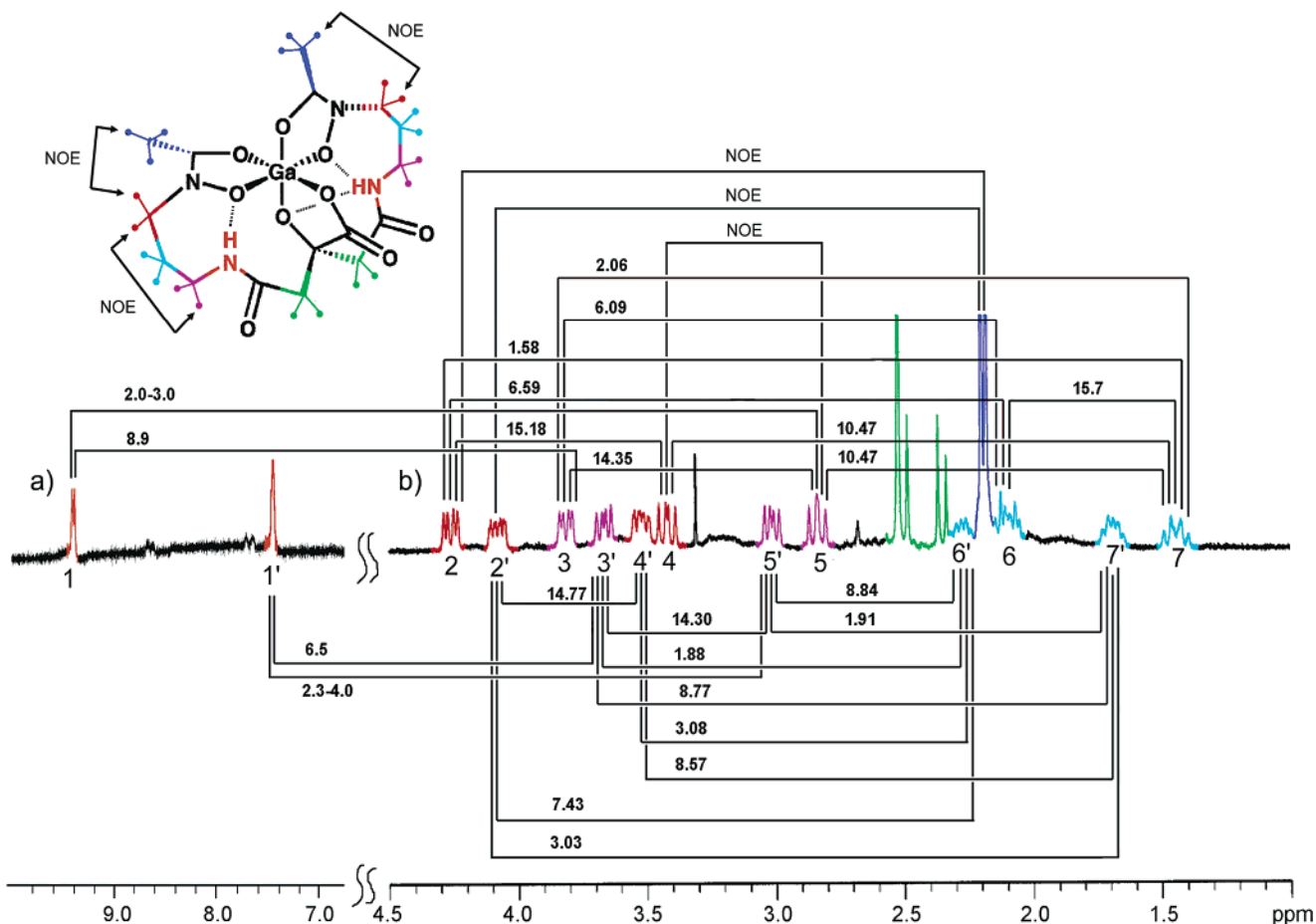


Figure 3. ^1H NMR spectrum of aqueous $\text{Na}[\text{GaSz}]$, $\text{pH} = 7$, $T = 25\text{ }^\circ\text{C}$: (a) WET-1D ^1H spectrum of the amide region in 10% D_2O ; (b) 1D ^1H spectrum in D_2O . Spin–spin connectivities, the corresponding coupling magnitudes, and the NOE contacts are indicated. Spin–spin coupling assignments for *chain I* are grouped above the spectral line and for *chain II*, below.

Table 1. ^1H NMR Peak Assignments of Ga Schizokinen Complex, GaSz^a

			Chain I						
resonance	δ	assignment	spin–spin couplings, Hz						
			2	3	4	5	6	7	
1	9.43	–NH–		8.9–8.7		~2			
2*	4.27	–CH ₂ –NOH			15.8		6.59	1.58	
3	3.81	–CH ₂ –NH				14.35	6.09	2.06	
4**	3.42	–CH ₂ –NOH	15.18					10.47	
5**	2.74	–CH ₂ –NH		14.35				10.47	
6	2.11	C–CH ₂ –C	6.59	6.09					15.7
7	1.45	C–CH ₂ –C	1.58	2.06	10.47	10.47	15.7		
			Chain II						
resonance	δ	assignment	spin–spin couplings, Hz						
			2'	3'	4'	5'	6'	7'	
1'	7.5	–NH–		6.5		2.3–4			
2'*	4.08	–CH ₂ –NOH			14.77		7.43	3.03	
3'	3.67	–CH ₂ –NH				14.3	1.88	8.77	
4'	3.52	–CH ₂ –NOH	14.77				3.08	8.57	
5'	3.02	–CH ₂ –NH		14.3			8.84	1.91	
6'	2.28	C–CH ₂ –C	7.43	1.88	3.08	8.84			~15
7'	1.69	C–CH ₂ –C	3.03	8.77	8.57	1.91	~15		

^a Spectra taken in D_2O at $\text{pD} = 7.5$. *NOE contact with terminal methyl hydrogens. **Weak NOE signal.

these hydrogen bonds, we studied dependencies of amide resonance chemical shifts on pD. The chemical shift of resonance 1' was slightly sensitive to solution pD in the alkaline region (pD ~ 11); in contrast resonance 1 did not change until the complete hydrolysis at pD ~ 12.

Kinetics of GaSz Racemization. The racemization rate was determined from DPGSE NOESY-1D spectra as a function of pD at 15 °C and 25 °C (Figure 8). There were two regimes of racemization, depending on acidity. At pD > 5 its rate was nearly constant, $k_{\text{rac}} \approx 1.4\text{ s}^{-1}$, and the ΔG^\ddagger profile vs T (Figure

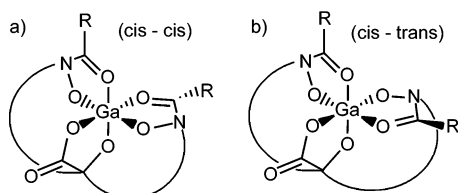


Figure 4. GaSz configurations, (a) *cis-cis* and (b) *cis-trans*.

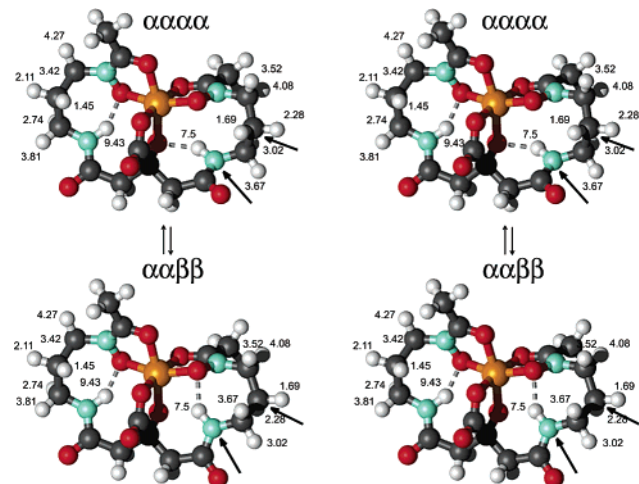


Figure 5. Structures of the two dominant GaSz conformations and ¹H NMR resonance assignments. Arrows show the groups with different ring-pucker arrangements in structures $\alpha\alpha\alpha\alpha$ and $\alpha\alpha\beta\beta$.

7) obtained from the measured rate constants clearly showed biphasic behavior. At $T < 28$ °C, ΔH^\ddagger was 25 ± 3 kcal M⁻¹ and ΔS^\ddagger was 25 ± 7 cal M⁻¹ K⁻¹. Above 28 °C the activation parameters sharply changed: ΔH^\ddagger became 17.1 ± 0.2 kcal M⁻¹ and ΔS^\ddagger dropped to a value of 0.3 ± 2.7 cal M⁻¹ K⁻¹. At $pD < 4$ the racemization sharply accelerated (Figure 8) and was first-order in $[D]^+$, where the rate constant k_{rac} could be represented as $k_{rac} = k_1 [D]^+ + k_0$, with $k_1 = (2.25 \pm 0.15) 10^4$ M⁻¹ s⁻¹, $k_0 = 1.47 \pm 0.15$ s⁻¹, $R^2 = 0.9924$.

Molecular Modeling of the Structures of GaSz and GaAf.

The geometry of the GaAf structure was approached by molecular modeling in several steps. Ab initio Hartree–Fock and DFT-optimized GaSz structures were examined for compatibility with the experimental vicinal spin–spin coupling values, the NOE contacts, and the dynamic features observed in the NMR spectra. Candidate structures for the core fragment of GaAf were chosen in *cis-cis* and *cis-trans* coordination geometries and with various 11-membered chelation ring pucker arrangements. The best geometries yielded a complete chemical shift assignment of the GaSz ¹H NMR spectrum shown in Figure 5. Finally, the favorable GaAf terminal alkyl chain orientations (Figure 6) were determined by analyzing the torsional energy profiles for the GaSz models extended with one terminal *trans*-1-propenyl and the *trans*-1-heptenyl tail.

GaSz Model Construction. We considered two GaSz configurations. The *cis-cis* configuration (Figure 4a), wherein both hydroxamate NO fragments are *cis* with respect to the ligand carboxyl group, appearing to be more relaxed in comparison to the *cis-trans* configuration (Figure 4b), in which the hydroxamate NO fragment on the right part of molecule is *trans*- with respect to the carboxyl group. A third, *trans-cis* configuration, was unstable in ab initio computations.

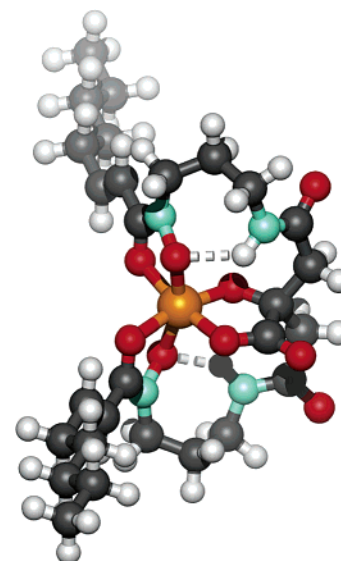


Figure 6. GaAf structure in $\alpha\alpha\beta\beta$ conformation of the core fragment and in one of the minimum-energy octenoyl tail conformations. Dashed lines denote the NH...O hydrogen bonds.

Models of GaSz with different 11-membered chelate ring-pucker conformations within both *cis-cis* and *cis-trans* geometries were built by changing orientations of the amide groups and the central methylene units on the two *N*-propylacetamido chains. The orientations of those groups were designated as α (“up”) or β (“down”).⁴⁷ As a reference, the molecular orientation was as shown in Figures 4 and 5.

Ab Initio Hartree–Fock and DFT Modeling. Calculation Strategy. The Hartree–Fock ab initio and DFT methods were explored for the modeling of GaSz structures. Geometry optimizations with B3LYP/6-31G(d) essentially reproduced the literature X-ray structure geometrical parameters of gallium hydroxamate complexes.^{48–52} By contrast, some of those parameters in the RHF/6-31G(d) gas-phase geometry-optimized structures deviated slightly from those known from literature.^{48–52} In particular, the hydroxamate C–O bond length in the RHF/6-31G(d) structures (1.24 Å) was ~ 0.03 Å shorter than is typical. However, the relative conformational energies were practically the same when obtained for both ab initio RHF/6-31G(d) and DFT B3LYP/6-31G(d) methods.⁵³ We conclude that a slight inaccuracy in the geometry predictions for the gallium

(47) The four-symbol combinations ($\alpha\alpha\alpha\alpha$, $\alpha\alpha\alpha\beta$, $\alpha\gamma\beta\alpha$, etc.) were used to define the various ring-pucker conformations of GaSz. The label characters reflect orientations of the four groups labeled as *i-iv* in Figure S25b: left-hand side methylene (*i*), left-hand side carbonyl (*ii*), right-hand side carbonyl (*iii*), and right-hand side methylene (*iv*) groups, in that order. An additional amide group conformation, “ γ ”, was introduced after we obtained the optimized structures. In that conformation the amide proton was hydrogen-bonded to the uncoordinated citrate central carboxyl oxygen, instead of one of the metal-bound oxygen atoms, as it was in all “ α ” and “ β ” conformations.

(48) Keys, A.; Barbarich, T. J.; Bott, S. G.; Barron, A. R. *J. Chem. Soc., Dalton Trans.* **2000w**, 577–588.

(49) Beissel, T.; Powers, R. E.; Raymond, K. N. *Angew. Chem., Int. Ed. Engl.* **1996**, *35*, 1084–1086.

(50) Dietrich, A.; Fidelis, K. A.; Powell, D. R.; Vanderhelms, D.; Engwilmot, D. L. *J. Chem. Soc., Dalton Trans.* **1991**, 231–239.

(51) Borgias, B. A.; Barclay, S. J.; Raymond, K. N. *J. Coord. Chem.* **1986**, *15*, 109–123.

(52) Dhungana, S.; White, P. S.; Crumbliss, A. L. *J. Am. Chem. Soc.* **2003**, *125*, 14760–14767.

(53) The relative GaSz conformation energies were almost the same when calculated with RHF/6-31G(d)/RHF/6-31G(d), RHF/6-31G(d)/B3LYP/6-31G(d), and B3LYP/6-31G(d)/B3LYP/6-31G(d) method combinations for the geometry optimization and the single point energy calculation

Table 2. GaSz *cis*–*trans* Conformation RHF/6-31G(d)//B3LYP-6-31G(d) Energies

conformation	Hartrees	kcal/mol
αααα	–3443.329 729	3.16
αααβ	–3443.338 531 ^a	0.0
ααβα	unstable ^b	
ααββ	unstable ^b	
αγαα	–3443.315 913	11.82
αγαβ	–3443.321 360	8.41
αγβα	unstable ^b	
αγββ	unstable ^b	
βααα	–3443.323 965	6.77
βααβ	–3443.328 808	3.74
βαβα	unstable ^b	
βαββ	unstable ^b	
ββαα	unstable ^b	
ββαβ	unstable ^b	
βββα	unstable ^b	
ββββ	unstable ^b	

^a B3LYP/6-31G(d)//B3LYP/6-31G(d) energy of this conformer is –3443.348535 Hartrees. ^b Geometry converged to that of another in the table or the Ga³⁺ center had lost its ligation to some of the chelating groups.

Table 3. GaSz Conformation Energies in *cis*–*cis* Configuration

conformation	B3LYP/6-31G(d) ^a		B3LYP/6-31G(d) dipole ^{a,b}	
	Hartrees	kcal/mol	Hartrees	kcal/mol
αααα	–3443.343320	0.03	–3443.355297	0.54
αααβ	unstable*			
ααγα	–3443.341621	1.09	–3443.346283	6.19
ααββ	–3443.343364	0	–3443.356151	0
αγαα	–3443.338458	3.08	–3443.343919	7.68
αβαβ	unstable*			
αγβα	–3443.338458	3.08	–3443.343919	7.68
αγββ	–3443.339718	2.29	–3443.345997	6.37
βααα	–3443.338223	3.23	–3443.352253	2.45
βααβ	unstable*			
βαγα	–3443.337988	3.37	–3443.342807	8.37
βαββ	–3443.339641	2.34	–3443.353064	1.94
βγαα	–3443.336341	4.41	–3443.348225	4.97
βββα	–3443.338592	2.99	–3443.348213	4.98
βγββ**	–3443.337257	3.83	–3443.345997	4.17
ββββ	–3443.339332	2.53	–3443.349505	4.17

^a Both structure optimization and single point energy calculations were done with the same method. ^b Onsager dipole solvent reaction field (SCRf) model, $a_0 = 5.80$ Å. *Geometry was found to converge to some other hexacoordinated structure listed in the table or (for *cis*–*trans* configuration) loose one of the hydroxamate Ga–O bonds during the geometry optimization. ***cis*–*cis* structure labeled βγββ strongly resembles structure ββββ with a slight difference of the amide group orientation; amide in βγββ is hydrogen bonded to the Ga-bound carboxyl oxygen instead of the carbonyl oxygen as in ββββ.

hydroxamates at the RHF level of theory was not accompanied by a deterioration of accuracy in the relative conformation energies.

Gas-Phase Calculations of GaSz. Thirteen unique conformations were found for the *cis*–*cis* geometry; three more were unstable. The *cis*–*trans* configuration yielded only six stable conformations, as it was considerably more demanding on the pucker of the right side *N*–*n*-propylacetamido fragment. The B3LYP/6-31G(d) energies for the corresponding structures of both configurations are presented in Tables 2 and 3. Several conformations of the *cis*–*cis* geometry had indistinguishable energies. The B3LYP/6-31G(d) conformation energies are nearly additive with respect to the orientations of the chosen conformation-defining groups (*i*–*iv* in Figure S25b), further confirming that such calculations produce chemically accurate energy values.

For the *cis*–*cis* geometry, the total energy was more sensitive to the pucker in the left *N*–*n*-propylacetamido chain. The changes in energy due to the pucker variations in the left and the right *N*–*n*-propylacetamido branches were 0.3–4.4 kcal/mol and 0–1.9 kcal/mol, respectively, and these contributions to the total energy were independent of each other to the precision of 1 kcal/mol. Also, the greater rigidity of the left *N*–*n*-propylacetamido branch was supported by the facts that its “αβ” conformation was unstable and the corresponding gallium hydroxamate five-membered ring was more distorted vs the other two five-membered chelation rings.

In the *cis*–*trans* geometry, the right *N*–*n*-propylacetamido chain (having the hydroxylamino oxygen in the *trans*- position with respect to the citrate carboxyl) was more conformationally constrained. Consequently, all structures with the right amide carbonyl in the “β” conformation were unstable and automatically converged to the “α” conformation. The “ββ” conformation of the left chain was also unstable. Energetic separations between the *cis*–*trans* GaSz conformations (3.1–8.6 kcal/mol) due to change of conformation on a single node (“α”, “β”, or “γ”) were typically larger than those for the *cis*–*cis* configuration (0–3.3 kcal/mol). Therefore, the computation provides compelling evidence of a diminished conformational freedom of the *cis*–*trans* GaSz configuration compared to the *cis*–*cis* geometry.

Onsager Model Solution Phase Calculations of GaSz. To investigate the effect of the aqueous medium on the GaSz structures and their energies, we used the Onsager dipole self-consistent reaction field (SCRf) model^{54,55} at the B3LYP/6-31G(d) level of theory. These calculations were confined to the *cis*–*cis* geometry, since that geometry proved to be preferable (see the following section). The cavity radius a_0 was chosen at 5.80 Å as determined by the molecular volume calculation in Gaussian98⁵⁶ for the gas-phase geometry optimized B3LYP/6-31G(d) *cis*–*cis* αααα conformation. That cavity radius and dielectric constant of 78.39 were then used in the SCRf calculations for all conformations. Calculated energies of the SCRf geometry-optimized structures are listed in Table 3. As expected for the Onsager theory, the overall energy trend is such that the change in the absolute energy upon placing the molecules into the dielectric continuum is proportional to the square of their dipole moments (Figure S21 and Table S1). Relative energies of most conformers have increased upon placement in the dielectric continuum with respect to the ground-state structures, only those energies of the βααα and βαββ conformers have slightly decreased. Importantly, the lowest-energy conformations in the gas phase remained the lowest-energy conformations in the SCRf solution phase calculations,

(54) Onsager, L. *J. Am. Chem. Soc.* **1936**, *58*, 1486–1493.

(55) Wong, M. W.; Frisch, M. J.; Wiberg, K. B. *J. Am. Chem. Soc.* **1991**, *113*, 4776–4782.

(56) Frisch, M. J.; Trucks, G. W.; Schlegel, H. B.; Scuseria, G. E.; Robb, M. A.; Cheeseman, J. R.; Zakrzewski, V. G.; Montgomery, J. J. A.; Stratmann, R. E.; Burant, J. C.; Dapprich, S.; Millam, J. M.; Daniels, A. D.; Kudin, K. N.; Strain, M. C.; Farkas, O.; Tomasi, J.; Barone, V.; Cossi, M.; Cammi, R.; Mennucci, B.; Pomelli, C.; Adamo, C.; Clifford, S.; Ochterski, J.; Petersson, G. A.; Ayala, P. Y.; Cui, Q.; Morokuma, K.; Malick, D. K.; Rabuck, A. D.; Raghavachari, K.; Foresman, J. B.; Cioslowski, J.; Ortiz, J. V.; Baboul, A. G.; Stefanov, B. B.; Liu, G.; Liashenko, A.; Piskorz, P.; Komaromi, I.; Gomperts, R.; Martin, R. L.; Fox, D. J.; Keith, T.; Al-Laham, M. A.; Peng, C. Y.; Nanayakkara, A.; Gonzalez, C.; Challacombe, M.; Gill, P. M. W.; Johnson, B.; Chen, W.; Wong, M. W.; Andres, J. L.; Gonzalez, C.; Head-Gordon, M.; Replogle, E. S.; Pople, J. A. *Gaussian 98*, version A.7; Gaussian, Inc.: Pittsburgh, PA, **1998**.

consistent with their dipole moments being one of the largest within the whole set of conformers.

Determination of Favorable Octenoyl Side-Chain Orientations in FeAf. Favorable orientations of Af octenoyl pendant side chains were investigated by analysis of the calculated torsional energy profiles for the two rotatable C–C bonds: one (C_{CO}–C_α) was modeled on the GaSz structure with one of the terminal methyl groups replaced by a 2-*trans*-methylvinyl group (inset in Figure S18), and the second (C_β–C_γ) was modeled on an analogous structure, modified with the 2-*trans*-propylvinyl group (inset in Figure S17).

In the minimum energy C_{CO}–C_α torsional orientation, the C=C bond is *cisoid coplanar* with respect to the hydroxamate carbonyl. The *transoid* orientation is very unfavorable due to a severe steric interaction of the vinyl group with the *n*-propyl moiety. Rotation of the vinyl group out of the hydroxamate plane is restricted by ~5 kcal/mol due to the loss of conjugation with the hydroxamate π-electron system. The most favorable orientation is in agreement with the NOE spectrum of GaAf (Figure S16) showing strong NOE signals between the vinyl α-protons (doublet at ~δ 6.38) and low-field methylene protons of the corresponding 1,3-diaminopropane fragment (multiplets at δ 4.47 and δ 4.35). The C_β–C_γ bond torsional energy profile (Figure S17) has two energetically indistinguishable global minima around the angles of ±60°. One of the minimum-energy conformations of the pendant GaAf octenoyl fragments is shown in Figure 6. The two octenoyl tails are clearly oriented in the opposite directions, separated by the average planar angle of ~130° (for all minimum-energy conformations), unlike the parallel side-chain arrangement in the phospholipid membrane molecules.

Vesicle Fusion Induced by FeAf. TEM experiments were performed to investigate the process of vesicle fusion in the presence of Af and FeAf. Upon incubation of DMPC small unilamellar vesicles (SUV) prepared as described in the literature²³ with 2.5 μM Af, some vesicle aggregation was apparent, but a large percentage (50%) of vesicles retained a normal structure (Figure S22). The fusion process was obviously enhanced in the presence of 2.5 μM FeAf, with almost 100% SUV (Figure S22) aggregated into large vesicle clusters and with a significant amount of broken vesicles. Therefore, we concluded that FeAf facilitates vesicle fusion and their disruption. That Af is considerably more hydrophobic than FeAf was shown by the significant change in octanol–water partition coefficient upon binding iron, 1.78 and 0.260, respectively.

Discussion

Synthesis. The general synthesis of acinetoferrin, schizokinen, and their analogues described here features the use of a new siderophore building block, the 1-*N*-benzoyloxy-1,3-diaminopropane bis-hydrochloride. The method minimizes the risk of iron contamination and could be adapted for solid phase and combinatorial preparations.

Coordination Geometry of GaSz. The preferred modes of hydroxamate coordination of GaSz and, thereby, GaAf were shown to be *cis–cis* in aqueous solution. The assignment became clear after inspection of the racemization-induced crosscorrelation and NOE-contact signals in the NOE spectra (Figures S15 and S16, respectively). Racemization can only exchange pro-*R* methylene group protons on the left side with

the pro-*S* methylene group protons on the right side. The two protons, one on *chain I* (resonance 2) and one on *chain II* (resonance 2'), displaying NOE contact with the corresponding terminal methyl group in Sz (Figures 3, S15, and Table 1), and the α-methylene group in Af (Figure S16), *do not exchange* upon racemization, and therefore must be both pro-*S* or both pro-*R*.

All conformations of the *cis–cis* configuration (Figures 5 and S23) except the βααα and βαββ strictly matched the above observations. The latter two structures have calculated gas-phase and SCRF energies of 2.6–3.2 kcal/mol and 1.94–2.45 kcal/mol above the ground state conformation, respectively, and therefore should not represent the GaSz structure at room temperature. By contrast, all conformations of the *cis–trans* configuration (Figures S24 and S25c) did not agree with the observed NOE and racemization exchange patterns. Therefore, only the *cis–cis* configuration is consistent with the experimental data.

Complete Structural ¹H Chemical Shift Assignment and Experimental Validation of the Favorable Conformations.

A first problem on the way to a full ¹H NMR resonance assignment was attributing the *chain I* and *chain II* resonances to the two *n*-propyl fragments in the *cis–cis* GaSz structure. Those two chains differ in the orientation of the corresponding hydroxamate group with respect to the α-hydroxy carboxyl moiety: one (the left side in Figure 4a) has the hydroxamate carbonyl *trans* to the citrate hydroxyl and the another (the right side in Figure 4a) is *cis*.

According to the NMR data, *chain I* is more rigid than *chain II* and must adopt a single staggered conformation of the propyl fragment. On the other hand, the gas phase and SCRF calculations showed that the two lowest-energy conformations, αααα and ααββ, have identical pucker arrangements for the left propyl fragment. Therefore *chain I* was assigned to the left side of the structure.

The next task toward a full ¹H NMR spectrum assignment was verification of observed ³J spin–spin couplings with the calculated GaSz geometries. The computed GaSz conformations had the Haasnoot-model⁵⁷ ³J vicinal coupling values for the left *n*-propyl chain in excellent agreement with the measured couplings on *chain I*. By contrast, none of the conformations had ³J vicinal coupling values that agreed well with the observed splittings on *chain II* (Table 4). The obviously averaged vicinal couplings observed in *chain II* (Figure 3 and Table 1) and the absence of a clear diaxial spin–spin coupling pattern for either of the *chain II* central methylene hydrogen atoms suggested a conformational mixture. Indeed, there was an excellent agreement between the experimental and *average* calculated ³J HCCH⁵⁷ and HNCH^{58–61} coupling constants (Table 4, columns 2 and 3) for the two lowest energy conformations (αααα and ααββ, Table 3 and Figure 5).

The NMR data in the amide region are also consistent with the αααα and ααββ GaSz conformations. Remarkably, the ab initio and DFT calculations predicted the intramolecular hy-

(57) Haasnoot, C. A. G.; Deleeuw, F.; Altona, C. *Tetrahedron* **1980**, *36*, 2783–2792.

(58) Demarco, A.; Llinas, M.; Wuthrich, K. *Biopolymers* **1978**, *17*, 637–650.

(59) Gavrilov, Y. D.; Solkan, V. N.; Bystrov, V. F. *Bull. Acad. Sci. USSR Div. Chem. Sci.* **1975**, *24*, 2368–2373.

(60) Aubry, A.; Giessner, C.; Cung, M. T.; Marraud, M.; Neel, J. *Biopolymers* **1974**, *13*, 523–536.

(61) Ramachandran, G. N.; Chandrasekaran, R.; Kopple, K. D. *Biopolymers* **1971**, *10*, 2113–2131.

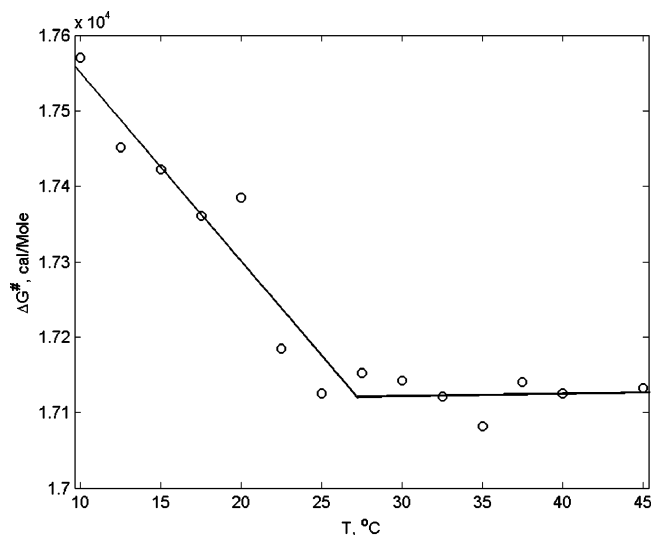
Table 4. Comparison of Measured ^1H Vicinal Spin–Spin Couplings with the Calculated Values for the Two Lowest Energy *cis–cis* GaSz Conformers

J_{k-y}	J_{obs} (Hz)	calculated couplings for energy-minimized structures		
		mean	$\alpha\alpha\alpha$	$\alpha\alpha\beta\beta$
Chain I				
6–4	-	0.8	0.8	0.9
7–4	10.47	12.1	12.2	11.9
6–2	6.59	6.4	6.5	6.3
7–2	1.58	1.1	1	1.1
5–6	--	1.1	1	1.1
3–6	6.09	6.3	6.4	6.1
5–7	10.47	12.2	12.3	12.1
3–7	2.06	1.2	1.1	1.2
1–3	8.8	5.57	5.0	6.15
1–5	2	4.15	6.29	2.4
Chain II				
2'–7'	3.03	3.3	4	2.5
2'–6'	7.43	8.3	12.5	4.1
4'–7'	8.57	7.4	2.2	12.5
4'–6'	3.08	3.3	4.5	2.2
7'–5'	1.91	1.0	0.7	1.3
7'–3'	8.77	9.7	7.2	12.1
6'–5'	8.84	8.8	11.7	5.9
6'–3'	1.88	0.9	0.7	1.1
1'–3'	6.5	5.9	7.0	4.81
1'–5'	3.2	4.36	2.37	6.35

drogen bonds between the amide hydrogen atoms and metal-bound hydroxamic and α -hydroxy carboxylic oxygen atoms (Figure S25). These hydrogen bonds form despite inducing an appreciable overall distortion of the tetrahedral carbon skeleton angles. The insensitivity of N–H resonance 1 chemical shift to pD, in contrast to that of resonance 1', indicates that N–H 1 undergoes a slower exchange with water, in agreement with the stronger corresponding intramolecular hydrogen bond, and thus, a higher ^1H chemical shift value (δ 9.43 for the resonance 1 vs 7.5 for the resonance 1', Figure 3 and Table 1). The calculated hydrogen bond lengths were also fully consistent with the relative magnitudes of the corresponding amide proton chemical shifts: the shorter hydrogen bond in *chain I* (1.77 Å on average, δ 9.43) and the ~ 0.1 Å longer one on *chain II* (1.87 Å on average, δ 7.5).

Thus, the *cis–cis* configuration of GaSz, conformations $\alpha\alpha\alpha$ and $\alpha\alpha\beta\beta$, best agree with the experiments and represent a structural model for the core fragment of the GaAf. Figure 5 shows a complete structural assignment of the methylene,⁶² the amide, and the terminal methyl ^1H NMR resonances for GaSz. As can be seen, the two structures are very similar in the overall arrangement. The left side has the same conformation in both structures. The ring-pucker conformation of the right side equilibrates between “ $\alpha\alpha$ ” and “ $\beta\beta$ ”. Both amide protons are hydrogen-bonded to one of the metal-coordinating oxygen atoms. The planar angle between the two hydroxamate acetyl C–C bonds in GaSz is 138° in the $\alpha\alpha\alpha$ structure and 120° in the $\alpha\alpha\beta\beta$ structure, having a strong effect on the geometry of a longer side-chain analogue, GaAf.

The Mechanism of GaSz Racemization. As discussed above, the dynamic racemization of GaSz was used to assign the preferred geometry as *cis–cis*. Ga^{3+} , having a d^{10} config-

**Figure 7.** Plot of GaSz racemization ΔG^\ddagger vs temperature, T . Circles: experimental data, solid line: plot of experimental data vs T at temperatures below and above 28°C , $\text{pH} = 7$.

uration, and thus no ligand field stabilization, forms labile complexes that racemize readily. There is only one known case of chiral gallium hydroxamate resolution, which was only achieved in aprotic solvent.⁶³ The racemization reported here ($k_{\text{rac}} \approx 1.4 \text{ s}^{-1}$) is an order of magnitude slower than the known racemizations of gallium tris-chelates.^{64–66} The unusually slow racemization GaSz is clearly related to the rigidity of the molecular framework and the two internal hydrogen bonds. Such intramolecular hydrogen bonds have been previously suggested to further stabilize the iron–siderophore complexes.^{67,68}

Clearly, there are two regimes of racemization, depending on the acidity (Figure 8). Above $\text{pH} 5$ this process is proton-independent and has a biphasic temperature dependence of ΔG^\ddagger (Figure 7). Only a mechanism with two or more *consecutive* steps can explain the L-shaped racemization ΔG^\ddagger profile vs T . Furthermore, the first step should be dissociative, manifested by the positive activation entropy. In the alternative case with two *competing* mechanisms, the low-entropy process would dominate in the low-temperature regime, resulting in the opposite ΔG^\ddagger profile vs T , where the smaller slope at lower T would be followed by a steeper slope at higher T . The activation parameters of the second step, rate limiting at slightly elevated temperatures, likely involves a trigonal-prismatic rearrangement, known as the Bailar twist,^{69–71} since the measured activation parameters, a modest ΔH^\ddagger and a low ΔS^\ddagger , are similar to the

- (63) Brumaghim, J. L.; Raymond, K. N. *J. Am. Chem. Soc.* **2003**, *125*, 12066–12067.
 (64) Karpishin, T. B.; Stack, T. D. P.; Raymond, K. N. *J. Am. Chem. Soc.* **1993**, *115*, 6115–6125.
 (65) Kersting, B.; Telford, J. R.; Meyer, M.; Raymond, K. N. *J. Am. Chem. Soc.* **1996**, *118*, 5712–5721.
 (66) Kersting, B.; Meyer, M.; Powers, R. E.; Raymond, K. N. *J. Am. Chem. Soc.* **1996**, *118*, 7221–7222.
 (67) Matsumoto, K.; Ozawa, T.; Jitsukawa, K.; Einaga, H.; Masuda, H. *Inorg. Chem.* **2001**, *40*, 190–191.
 (68) Tor, Y.; Libman, J.; Shanzer, A.; Felder, C. E.; Lifson, S. *J. Am. Chem. Soc.* **1992**, *114*, 6661–6671.
 (69) Casanova, D.; Cirera, J.; Llunell, M.; Alemany, P.; Avnir, D.; Alvarez, S. *J. Am. Chem. Soc.* **2004**, *126*, 1755–1763.
 (70) Montgomery, C. D.; Shorrocks, C. J. *Inorg. Chim. Acta* **2002**, *328*, 259–262.
 (71) It is clear that the analogue of the Bailar twist mechanism (Figure S27 a and b), if it is not preceded by dissociation of at least one chelating group, cannot be operative in the GaSz epimerization. Such a process requires rotation of all the chelating groups in the same direction, thus minimizing

(62) The citrate methylene ^1H NMR resonances were the only signals not reliably assigned to a particular conformation, but it is likely that the ab-quartet centered at δ 2.45 belongs to the conformationally restrained *chain I*, and the singlet at δ 2.55 to the more flexible and equilibrating *chain II*.

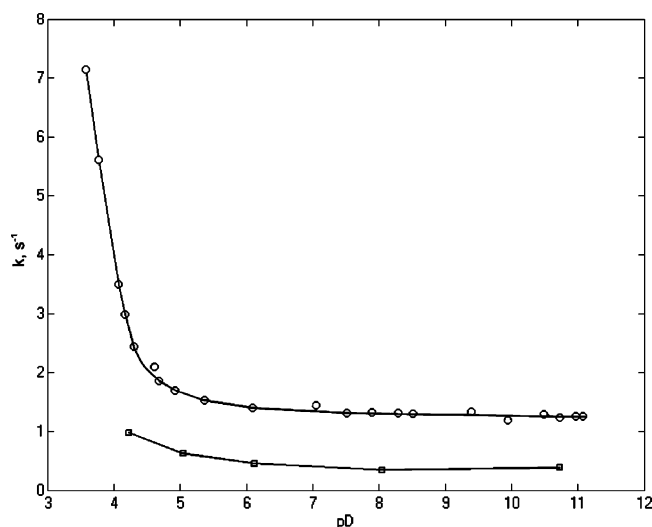


Figure 8. GaSz racemization rate constant vs pD: circles: 25 °C, squares: 15 °C.

values observed for such a mechanism for gallium catecholates (Figure 10),^{65,66,72} 8-hydroxyquinolinates,⁷³ and acetylacetonates.⁷⁴

The dissociation in the first step at pH > 5 should occur at the α -hydroxy carboxylate position, rather than at the hydroxamate position, since the latter is a much stronger ligand. Further, the dissociation is most likely to occur at the carboxylate position rather than the alkoxide position,⁷⁵ since there is no pH dependence for this process at pH > 5 and there is a strong evidence⁷⁶ that the carboxylate is a much more labile ligand to gallium.

Below pH 4, the marked first-order [H⁺] dependence was assigned to complete dissociation of the α -hydroxy-carboxyl moiety followed by a more facile rearrangement of the bis-hydroxamate intermediate. It is known that at pH \sim 2–3 the ionic charge of FeSz switches from -1 to $+1$ upon simultaneous acceptance of two protons, while the resulting complex is best described as a bis-hydroxamate.⁴⁰

Geometry of the Alkyl Tails of GaAf and Biological Implications. The unusual feature of the Af molecule is the presence of two unsaturated side chains conjugated to the hydroxamate carbonyl groups. Significantly, for all reasonable structures of GaAf and GaSz, the two substituent alkenyl or alkyl groups are held rigidly in an antiparallel arrangement at an angle of about 130°. The C_{CO}–C _{α} bond of the octenoyl fragment is rotationally constrained by the π -electronic conjugation of the vinyl fragments with the hydroxamate carbonyl

the unfavorable nonbonding interactions in the transition state. Such a process, if applied to the GaSz, would lead to an unstable trans–trans isomer (Figure S27 b). Thus, a nondissociative epimerization of GaSz would require a more complex and energetically prohibitive pathway.

- (72) Raymond, K. N.; Dertz, E. A.; Kim, S. S. *Proc. Natl. Acad. Sci. U.S.A.* **2003**, *100*, 3584–3588.
- (73) Gromova, M.; Jarjayes, O.; Hamman, S.; Nardin, R.; Beguin, C.; Willem, R. *Eur. J. Inorg. Chem.* **2000**, 545–550.
- (74) Hutchison, J. R.; Gordon, J. G.; Holm, R. H. *Inorg. Chem.* **1971**, *10*, 1004–1017.
- (75) Additional evidence that the dissociation of carboxylate is favorable was obtained by ab initio modeling of the dissociative transition state geometry at the RHF/3-21G level of theory (Figure S26). In the transition state Ga³⁺ essentially has tetragonal prismatic coordination with the two hydroxamate five-membered chelation rings in a nearly parallel arrangement. This transition state geometry permits a simultaneous binding of an additional ligand, such as H₂O, to the distal part of the molecule further stabilizing the transition state compared to the nondissociative mechanism.
- (76) Hawkes, G. E.; O'Brien, P.; Salacinski, H.; Motevalli, M.; Abrahams, I. *Eur. J. Inorg. Chem.* **2001**, 1005–1011.

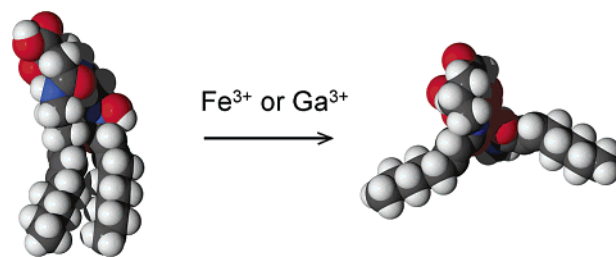


Figure 9. Change of Af conformation upon coordinating the metal ion.



Figure 10. Dissociative mechanism of the GaSz epimerization.

groups and the steric repulsion from the corresponding n -diaminopropyl fragments. The C _{β} –C _{γ} bond has two energetically equivalent favorable torsional angles. The resulting GaAf model (Figures 6 and 9) shows that the two *trans*-octenoyl groups are oriented in the opposite directions. These results indicate a significant structural reorganization of Af upon metal binding, since apo-Af can adopt many relaxed structures with phospholipidlike parallel arrangements of the lipophilic side chains while GaAf clearly cannot (Figure 9).

Trivalent gallium and iron citrates have very similar structures and share the same bidentate coordination mode with the α -hydroxy carboxylic moiety.^{76,77} Such structural similarity between Fe³⁺ and Ga³⁺ complexes is typical, for example, for tripodal salicylate-based ligands⁷⁸ and has been used in structural studies of several siderophores.^{79–81} Thus, we anticipate that FeAf and FeSz will have structures very similar to their gallium analogues. The large 8-fold change in partition coefficient upon binding iron indicates that Af is considerably *more* hydrophobic than FeAf, despite the facts that metal binding buries six hydrophilic oxygen atoms and there is no net change in molecular charge. We suggest that the skewed orientation of the octenoyl side chains that is enforced by iron binding is the origin of this change. Significantly, a similar change in apparent hydrophobicity upon iron binding was reported by us recently for the amphiphilic marine siderophore, marinobactin E,²³ suggesting that such differences are part of a larger iron acquisition strategy. Thus, membrane binding and lipid trafficking would provide directed avenues for iron extraction and delivery. The facility with which FeAf was observed to disrupt phospholipid vesicles, despite its greater hydrophilicity, and ongoing studies of membrane binding and permeability of a range of amphiphilic siderophores support this view.⁸²

- (77) Matzapetakis, M.; Raptopoulou, C. P.; Tsohos, A.; Papaefthymiou, V.; Moon, N.; Salifoglou, A. *J. Am. Chem. Soc.* **1998**, *120*, 13266–13267.
- (78) Cohen, S. M.; Petoud, S.; Raymond, K. N. *Inorg. Chem.* **1999**, *38*, 4522–4529.
- (79) Wasielewski, E.; Atkinson, R. A.; Abdallah, M. A.; Kieffer, B. *Biochemistry* **2002**, *41*, 12488–12497.
- (80) Atkinson, A. R.; Din, A. L. M. S.; Keiffer, B.; Lefevre, J.-F.; Abdallah, M. A. *Biochemistry* **1998**, *37*, 15965–15973.
- (81) Stephan, H.; Freund, S.; Meyer, J. M.; Winkelmann, G.; Jung, G. *Liebigs Ann. Chem.* **1995**, 43–48.
- (82) Our preliminary results show rapid paramagnetic NMR line broadening of DMPC choline methyl groups on the interior surface of the DMPC small unilamellar vesicles upon mixing with FeAf solution. This indicates that FeAf is capable of rapidly diffusing across the lipid layers. A further account of these phenomena will be reported elsewhere.

Experimental Section

Synthesis. Solvents were freshly distilled prior to use. Sephadex LH-20 and G-10 was obtained from the Sigma Chemical Company. Silica gel 60 was purchased from Sorbent Technologies. Crotonyl chloride, *trans*-2-octenoic acid, and *trans*-2-dodecenoic acid were purchased from Lancaster Synthesis, anhydrous citric acid from Fisher Scientific, 1,2-Dimyristoyl-*sn*-Glycero-3-Phosphocholine (DMPC) from Avanti Lipids, and all other reagents from Aldrich Chemicals. All reagents were used without further purification, unless otherwise noted.

1-*N*-Benzoyloxy-1,3-diaminopropane Dihydrochloride (2). *N*-(Benzoyloxy)-3-(tert-butoxycarbonylamino)propylamine⁴³ (3.7 g, 12.5 mmol) was dissolved in 250 mL of ether and 50 mL of methanol. Anhydrous HCl was bubbled through the solution for 1 h without cooling. After removal of the solvent, 3.1 g of **2** was collected as a white solid (92% yield). The presence of methanol was essential for complete removal of the Boc group.

¹H NMR (CD₃OD) δ: 2.16 (m, 2H, CH₂), 3.18 (t, 2H, CH₂), 3.57 (t, 2H, CH₂), 7.57 (d, 2H, aromatic), 7.75 (m, 1H, aromatic), 8.1 (m, 2H, aromatic).

¹³C NMR (CD₃OD) δ: 23.41 (CH₂), 39.15 (CH₂), 49.20 (CH₂), 130.28 (CH, aromatic), 130.95 (CH, aromatic), 134.37 (CH, aromatic), 135.93 (C, aromatic), 166.38 (CO, carbonyl).

Anal. Calcd for C₁₀H₁₆Cl₂N₂O₂: C, 44.96; H, 6.04; Cl, 26.54; N, 10.49. Found: C, 44.70; H, 5.94; Cl, 26.41; N, 10.24.

2-*tert*-Butyl-1,3-((3-*N*-benzoyloxy)propyl)diamide Citrate (3). Protected di-*N*-hydroxysuccinimidyl citrate⁴² **1**, (3 g, 6.78 mmol) was dissolved in 50 mL of dry acetonitrile. To this was added 3.27 g (12.2 mmol) of solid **2**. After that, 5.47 mL (39.3 mmol) of triethylamine in 50 mL of dry acetonitrile was added dropwise to the stirred above suspension. The reaction mixture was stirred at 25 °C for 1 h. After removing the solvent the reaction mixture was partitioned between chloroform and water, and the organic layer evaporated to dryness. The crude product was purified by silica column chromatography with 4%CH₃OH/CHCl₃ used as eluent. Yield: 2.22 g (55%).

¹H NMR (CDCl₃) δ: 1.46 (s, 9H, *tert*-butyl), 1.83 (m, 4H, CH₂), 2.65 (ab-quartet, 4H, citrate CH₂), 3.2 (t, 4H, CH₂), 3.41 (t, 4H, CH₂), 6.9 (t, 2H, amide), 7.45 (t, 4H, aromatic), 7.59 (t, 2H, aromatic), 8.00 (d, 4H, aromatic).

¹³C NMR (CDCl₃) δ: 26.73 (CH₂, 1,3-diaminopropane), 27.49 (CH₃), 36.8 (CH₂), 43.63 (CH₂), 49.53 (CH₂, 1,3-diaminopropane), 74.00 (C, tertiary), 82.10 (C, tertiary), 128.10, 128.24, 128.97, 133.07, 166.33, 170.06, 172.58.

HRMS (EI) *m/z* calcd for C₃₀H₄₁N₄O₉ (M⁺): 601.2874. Found: 601.2898.

2-*tert*-Butyl-1,3-((3-*N*-benzoyloxy-3*N*-acyl)propyl)diamide Citrate (4). **General Procedure.** 2-*tert*-Butyl-1,3-((3-*N*-benzoyloxy)propyl)-diamide citrate **3**, 0.9 g (1.5 mmol), was dissolved in 20 mL of dry dichloromethane. The solution was heated to reflux temperature and 2.1 equiv of acyl chloride in 10 mL of dry dichloromethane was added. The reaction mixture was refluxed for 1 h. After evaporating the solvent the oily residue was subjected to column chromatography (silica/ethyl acetate–hexanes). Yields after purification were 0.82 g (80%) for **4a**, 0.98 g (77%) for **4b**, 0.82 g (75%) for **4c**, and 1.12 g (78%) for **4d**.

4a: ¹H NMR (CD₃OD) δ: 1.42 (s, 9H, *tert*-butyl), 1.83 (m, 4H, CH₂), 2.05 (broad s, 6H, CH₃), 2.6 (ab-quartet, 4H, citrate CH₂), 3.25 (t, 4H, CH₂), 3.87 (t, 4H, CH₂), 7.59 (t, 4H, aromatic), 7.78 (t, 2H, aromatic), 8.15 (d, 4H, aromatic).

¹³C NMR (CDCl₃) δ: 20.32 (CH₃), 26.94, 27.80, 36.36, 44.11, 45.80, 73.94, 82.74, 126.45, 129.02, 130.05, 134.73, 164.57, 169.93, 172.77.

4b: ¹H NMR (CDCl₃) δ: 0.82 (t, 6H, CH₃), 1.25 (m, 8H, CH₂), 1.40 (m, 4H, CH₂), 1.48 (s, 9H, *tert*-butyl), 1.87(m, 4H, CH₂), 2.15 (m, 4H, CH₂), 2.75 (ab-quartet, 4H, citrate CH₂), 3.40 (m, 4H, CH₂), 3.93 (m, 4H, CH₂), 6.04 (d, 2H, CH), 7.02(m, 2H, CH), 7.52 (t, 4H, aromatic), 7.69 (t, 2H, aromatic), 8.12(d, 4H, aromatic).

¹³C NMR (CDCl₃) δ: 13.92, 22.36, 27.03, 27.73, 27.80, 31.22, 32.45, 36.39, 44.07, 46.15, 73.98, 82.66, 117.79, 126.53, 129.01, 130.90, 134.65, 149.89, 164.63, 166.91, 169.99, 172.67.

ESI–MS: *m/z* 849 (MH⁺), 871 (MNa⁺).

4c: ¹H NMR (CDCl₃) δ: 1.48 (s, 9H, *tert*-butyl), 1.85(m, 10H, CH₃ and CH₂), 2.70 (ab-quartet, 4H, citrate CH₂), 3.37 (m, 4H, CH₂), 3.93 (m, 4H, CH₂), 6.08 (d, 2H, CH), 7.05(m, 2H, CH), 7.52 (t, 4H, aromatic), 7.68 (t, 2H, aromatic), 8.11(d, 4H, aromatic).

¹³C NMR (CDCl₃) δ: 18.32, 27.01, 27.80, 36.41, 44.02, 46.15, 73.97, 82.66, 119.28, 126.49, 129.02, 130.11, 134.68, 144.99, 164.63, 166.63, 170.01, 172.67.

ESI–MS: *m/z* 759 (MNa⁺).

4d: ¹H NMR (CDCl₃) δ: 0.82 (t, 6H, CH₃), 1.23 (m, 24H, CH₂), 1.39 (m, 4H, CH₂), 1.48 (s, 9H, *tert*-butyl), 1.87(m, 4H, CH₂), 2.17 (m, 4H, CH₂), 2.71 (ab-quartet, 4H, citrate CH₂), 3.40 (m, 4H, CH₂), 3.96(m, 4H, CH₂), 6.08(d, 2H, CH), 7.05m, 2H, CH), 7.12 (t, 2H, amide), 7.57 (t, 4H, aromatic), 7.73 (t, 2H, aromatic), 8.14(d, 4H, aromatic).

2-*tert*-Butyl-1,3-((3-*N*-hydroxy-3*N*-acyl)propyl)diamide Citrate (5). **General Procedure.** A 0.65 mmol amount of **2** was dissolved in 20 mL of methanol in a polyethylene container loaded with a Teflon-coated magnetic stirrer. The solution was cooled to 0 °C and 287 μL of 5 N NaOH (2.2 equiv) in water was added. After 5 min 287 μL of 5 N HCl was added. Methanol and water were removed on a rotary evaporator and the residue was subjected to column chromatography (methanol/chloroform) on pretreated silica as described in ref 43. Yields after purification were 80%, (94%) for **5b**.

5a: ¹H NMR (CD₃OD) δ: 1.48 (s, 9H, *tert*-butyl), 1.80 (t, 4H, CH₂), 2.10 (s, 6H, CH₃), 2.62 (ab-quartet, 4H, citrate CH₂), 3.19 (t, 4H, CH₂), 3.62 (t, 4H, CH₂).

¹³C NMR (CD₃OD) δ: 20.44, 27.66, 28.33, 37.74, 46.26, 46.66, 75.32, 83.77, 172.11, 173.86, 174.61.

5b: ¹H NMR (CD₃OD) δ: 0.90 (t, 6H, CH₃), 1.35 (m, 8H, CH₂), 1.48 (m, 13H, CH₂ and *tert*-butyl), 1.82(m, 4H, CH₂), 2.23 (m, 4H, CH₂), 2.65 (ab-quartet, 4H, citrate CH₂), 3.20 (m, 4H, CH₂), 3.72 (t, 4H, CH₂), 6.61 (d, 2H, CH), 6.85 (m, 2H, CH).

¹³C NMR (CD₃OD) δ: 14.49, 23.61, 27.72, 28.32, 29.05, 29.29, 32.61, 33.52, 37.82, 45.19, 46.99, 75.28, 83.77, 120.51, 148.36, 168.61, 172.15, 174.49, 176.91.

ESI–MS: *m/z* 641 (MH⁺), 663 (MNa⁺).

5c: ¹H NMR (CD₃OD) δ: 1.48 (s, 9H, *tert*-butyl), 1.82 (t, 4H, CH₂), 1.90 (ab-quartet, 6H, CH₃), 2.64 (ab-quartet, 4H, citrate CH₂), 3.18 (t(broad), 4H, CH₂), 3.7 (t(broad), 4H, CH₂), 6.63(d(broad), 4H, CH), 6.86(m, 2H, CH).

¹³C NMR (CD₃OD) δ: 18.44, 27.69, 28.29, 37.76, 45.29, 46.89, 75.27, 83.74, 121.96, 143.36, 168.62, 172.12, 174.52, 176.87.

ESI–MS: *m/z* 529 (MH⁺), 551 (MNa⁺).

5d: ¹H NMR (CD₃OD) δ: 0.90 (t, 6H, CH₃), 1.32 (m, 28H, CH₂), 1.45 (s, 9H, *tert*-butyl), 1.82(m, 4H, CH₂), 2.23 (m, 4H, CH₂), 2.62 (ab-quartet, 4H, citrate CH₂), 3.19 (m, 4H, CH₂), 3.73 (t, 4H, CH₂), 6.61 (d, 2H, CH), 6.85 (m, 2H, CH).

ESI–MS: *m/z* 753 (MH⁺), 775 (MNa⁺).

Schizokinen, Acinetoferrin, and Analogues (6a–d). *tert*-Butyl deprotection was effected as in Wang and Phanstiel,⁴³ with TFA at room temperature. After the deprotection was complete, TFA was removed on a rotovap and finally under high vacuum. No heating was used at any time during TFA removal. Compounds **6b** and **6d** could be separated from the residual TFA by partition between the water and the chloroform and evaporation of the chloroform phase, while compounds **6a** and **6c** could be separated by repetitive lyophilization from aqueous solutions. Compounds **6a** and **6c** were purified by sephadex G-10 gel filtration, eluting with water, compounds **6b** and **6d** – by sephadex LH-20 eluted with CHCl₃:ethanol (15:85).

6a (Sz): ¹H NMR (D₂O) δ: 1.69 (m, 4H, CH₂), 2.1 (s, 6H, CH₃), 2.61(ab-quartet, 4H, citrate CH₂), 3.17 (m, 4H, CH₂), 3.63 (t, 4H, CH₂).

¹³C NMR (CD₃OD) δ : 20.43, 27.72, 37.76, 46.28, 46.64, 75.36, 172.17, 173.85, 177.21.

6b (Af): ¹H NMR (CD₃OD) δ : 0.94 (t, 6H, CH₃), 1.35 (m, 8H, CH₂), 1.48 (m, 4H, CH₂), 1.82 (m, 4H, CH₂), 2.14 (m, 4H, CH₂), 2.69 (ab-quartet, 4H, citrate CH₂), 3.20 (t, 4H, CH₂), 3.73 (t, 4H, CH₂), 6.62 (broad d, 2H, CH), 6.83 (m, 2H, CH).

¹³C NMR (CD₃OD) δ : 14.42, 23.55, 27.35, 29.07, 29.32, 32.65, 33.53, 37.77, 45.23, 47.04, 75.28, 120.54, 148.42, 168.58, 172.31, 177.25.

Anal. Calcd for C₂₈H₄₈N₄O₉: C, 57.52; H, 8.27; N, 9.58; O, 24.63. Found: C, 57.60; H, 8.42; N, 9.34.

6c: ¹H NMR (CD₃OD) δ : 1.81 (m, 4H, CH₂), 1.93 (d, 6H, CH₃), 2.70 (ab-quartet, 4H, citrate CH₂), 3.20 (t, 4H, CH₂), 3.61 (t, 4H, CH₂), 6.63 (d, 2H, CH), 6.85 (m, 2H, CH).

¹³C NMR (CD₃OD) δ : 18.43, 27.65, 37.78, 45.24, 46.87, 75.25, 121.98, 143.32, 168.67, 172.24, 177.25.

ESI-MS: *m/z* 473 (MH⁺), 495 (MNa⁺).

6d: ¹H NMR (CD₃OD) δ : 0.90 (t, 6H, CH₃), 1.29 (m, 24 H, CH₂), 1.47 (m, 4H, CH₂), 1.82 (m, 4H, CH₂), 2.24 (m, 4H, CH₂), 2.68 (ab-quartet, 4H, citrate CH₂), 3.20 (t, 4H, CH₂), 3.70 (t, 4H, CH₂), 6.62 (broad d, 2H, CH), 6.84 (m, 2H, CH).

¹³C NMR (CD₃OD) δ : 14.62, 23.85, 27.76, 30.44, 30.55, 30.65, 30.78, 33.16, 33.84, 45.26, 47.31, 75.25, 120.53, 148.34, 168.62, 172.28, 177.19.

Anal. Calcd for C₃₆H₆₄N₄O₉: C, 62.04; H, 9.26; N, 8.04; O, 20.66. Found: C, 62.30; H, 9.55; N, 7.70.

Iron Acinetoferrin Complex (FeAf). Acinetoferrin **6c**, 1 equiv from 2 mM solution in 100 mM pH 7.4 HEPES (aqueous + 20% vol. of DMF or methanol to solubilize the acinetoferrin) buffer was mixed with 1 equiv of 2 mM (in Fe concentration) solution of ferric ammonia citrate in 100 mM pH 7.4 HEPES buffer and kept in a dark place at 25 °C for 24 h to allow for slow iron acquisition from ferric citrate clusters to complete.

Iron and Gallium Schizokinen Complexes (FeSz and GaSz). Schizokinen **6a**, 1 equiv from 2 mM aqueous solution was mixed with 1 equiv of an aqueous solution of ferric nitrate (or GaBr₃). The resulting solution was slowly neutralized by aqueous NaOH.

NMR Spectroscopy. All NMR spectra were recorded on Varian, Inc. 300, 400, and 500 MHz instruments. Deuterated solvents were purchased from Cambridge Isotope Laboratories, Inc. The ¹H 1D, COSY and NOESY spectra of GaSz were recorded in D₂O using conventional pulse sequences, and in a 9:1 H₂O:D₂O mixture using the corresponding pulse sequences modified with a WET water suppression pulse train.⁸³ GaSz racemization rates were measured with a NOESY-1D experiment in H₂O:D₂O 1:1 without solvent suppression using a double pulsed field gradient spin-echo (DPFGSE) selective multiplet excitation technique.⁴⁵ The methylene proton signal at δ 1.5 was selectively inverted and integral intensities of that multiplet and of a signal at δ 2.2 were recorded as a function of mixing time. The mixing time was within a range of 0.025–0.5 s. The sample pH was adjusted by adding small volumes (~10 μ L) of 0.1M DCl or NaOD solutions into the sample NMR tube and the pD was determined with an Aldrich NMR pH electrode. A 0.2 pH unit correction was applied to a pH meter reading to get the sample acidity instead of the suggested 0.4 since the latter value was determined for the pure D₂O solutions.⁸⁴

(83) Smallcombe, S. H.; Patt, S. L.; Keifer, P. A. *J. Magn. Reson., Ser. A* **1995**, *117*, 295–303.

The racemization rate constant was determined by fitting the temporal buildup of the exchange peak and the parent peak integral intensity ratio to a quadratic polynomial $a t^2 + b t$. The fitting parameter b was used for the rate constant value. The quadratic polynomial produced better fitting results than linear because the initial linear buildup period was too short. The ΔG^\ddagger for the dynamic racemization of GaSz was calculated by the Eyring equation using the determined rate constants in the temperature range of 10–45 °C at pD = 8.5.

Computations. The Gaussian 98⁵⁶ package was used for all computations. All torsional angle energy profiles and structural geometry optimizations were performed with RHF/6-31G(d) and B3LYP/6-31G(d)^{85–87} methods. Solution-phase computations were done with the Onsager dielectric continuum SCRF model^{54,55} at the continuum dielectric constant value of 78.39. The cavity radius $a_0 = 5.80$ Å was used as determined by the molecular volume calculation in Gaussian98. The molecular structure figures were prepared with the MolMol software.⁸⁸

Transmission Electron Microscopy. TEM images (Figure S22) were obtained with a JEOL 100C electron microscope using uranyl acetate (1.5 wt %) as the negative staining reagent. Freshly prepared 1,2-dimyristoyl-*sn*-glycero-3-phosphocholine (DMPC) SUV (0.05 mM, final concentration) was incubated for 12 h at 25 °C with blank buffer, **Af** (1:20, final molar ratio between apo-**Af** and DMPC) and ferric-acinetoferrin, **FeAf** (1:20, final molar ratio between **FeAf** and DMPC). A thin layer of mixed solution was then deposited onto a gold-coated grid. After being stained by aqueous uranyl acetate (1.5 wt %), the grid was dried in the air at room temperature for 15 min and then subjected to TEM image analysis. DMPC SUV in the absence of either **Af** or **FeAf** could be distributed homogeneously on the gold-coated grid, while DMPC SUV incubated with either **Af** or **FeAf** exhibited a heterogeneous distribution. Therefore, the images of the latter were recorded by selecting vesicle-aggregated regions. Partition coefficients were determined at 25 °C by the standard octanol–water procedure.

Acknowledgment. We thank Prof. Robert Pascal and Dr. Andrzej Jarzecki for helpful discussions on quantum calculations, Dr. Istvan Pelczer and Dr. Carlos Pacheco for assistance with the NMR experiments, and Dr. Joseph Goodhouse for assistance with TEM imaging. Financial support of this research by the National Science Foundation (CHE-0221978), through the Environmental Molecular Science Institute (CEBIC) at Princeton University is gratefully acknowledged.

Supporting Information Available: Mass and NMR spectra, charts with calculated torsion energy profiles, TEM images, images and coordinate tables of calculated structures, table with calculation parameters, and a scheme of the GaSz epimerization mechanism. This material is available free of charge via the Internet at <http://pubs.acs.org>.

JA048145J

(84) Glasoe, P. K.; Long, F. A. *J. Phys. Chem.* **1960**, *64*, 188–190.

(85) Becke, A. D. *Phys. Rev. A* **1988**, *38*, 3098–3100.

(86) Lee, C. T.; Yang, W. T.; Parr, R. G. *Phys. Rev. B* **1988**, *37*, 785–789.

(87) Vosko, S. H.; Wilk, L.; Nusair, M. *Can. J. Phys.* **1980**, *58*, 1200–1211.

(88) Koradi, R.; Billeter, M.; Wuthrich, K. *J. Mol. Graphics* **1996**, *14*, 51–55.